Antarctic Science 15 (1): 41–46 (2003) © Antarctic Science Ltd Printed in the UK DOI: 10.1017/S0954102003001044

M_2 tidal dynamics in the Ross Sea

ROBIN ROBERTSON*, AIKE BECKMANN and HARTMUT HELLMER

Alfred-Wegener-Institüt für Polar- und Meeresforschung, Postfach 12 0161, D-27515 Bremerhaven, Germany
**current address: Lamont-Doherty Earth Observatory, Columbia University, Palisades, NY 10964, USA*
rroberts@ldeo.columbia.edu

Abstract: In certain regions of the Southern Ocean, tidal energy is believed to foster the mixing of different water masses, which eventually contribute to the formation of deep and bottom waters. The Ross Sea is one of the major ventilation sites of the global ocean abyss and a region of sparse tidal observations. We investigated M_2 tidal dynamics in the Ross Sea using a three-dimensional sigma coordinate model, the Regional Ocean Model System (ROMS). Realistic topography and hydrography from existing observational data were used with a single tidal constituent, the semi-diurnal M_2. The model fields faithfully reproduced the major features of the tidal circulation and had reasonable agreement with ten existing tidal elevation observations and forty-two existing tidal current measurements. The differences were attributed primarily to topographic errors. Internal tides were generated at the continental shelf/slope break and other areas of steep topography. Strong vertical shears in the horizontal velocities occurred under and at the edges of the Ross Ice Shelf and along the continental shelf/slope break. Estimates of lead formation based on divergence of baroclinic velocities were significantly higher than those based on barotrophic velocities, reaching over 10% at the continental shelf/slope break.

Received 13 February 2002, accepted 30 July 2002

Key words: Antarctica, internal tides, polar, tides

Introduction

Barotrophic and baroclinic tides play significant roles in ocean mixing (Munk & Wunsch 1998, Muench *et al*. 2002) and in the ocean-atmosphere heat transfer (Padman & Kottmeier 2000, Robertson 2001b). Barotrophic tides increase benthic mixing through higher benthic shear, and baroclinic tides increase mid-water column mixing through shear instabilities. In the Antarctic seas, mixing along the continental slope can affect formation of deep and bottom waters and their ventilation. In addition, mixing has the potential to affect the heat transport from the Warm Deep Water to the surface ice and influence the ice cover (McPhee *et al*. 1996, Muench *et al.* 2002, Beckmann *et al.* 2001). As early as the 1800s, it was recognized that tides induce lead formation in the sea ice due to convergence and divergence of the velocities (Nansen 1898). The lead formation then affects the ocean-atmosphere heat transfer. Thus, through multiple mechanisms, tides have the capability to influence mixing and heat transfer in the Ross Sea. In order to understand and quantify their contribution, the tidal dynamics must first be understood.

Tidal observations for the Ross Sea are rather sparse (dots and triangles in Fig. 1), so models have been used to fill in data gaps and provide estimates of the tidal dynamics. The barotrophic tides in the Ross Sea have been modelled by MacAyeal (1984) and Padman and others (Padman & Kottmeier 2000, Padman *et al.* 2003). However, the vertical structure has not been addressed. Our goal was to investigate the three-dimensional M_2 tidal dynamics in the Ross Sea using the Regional Ocean Modeling System (ROMS), which is described in the next section. The model results are given and compared with the existing observations in the results section. Implications of the model results are discussed in the final section of the paper.

Model description

Model

Terrain-following models, such as the Princeton Ocean Model (POM) and ROMS, are preferable for simulating regions with widely varying topography due to their more realistic representations of the topography and benthic boundary layer with fewer vertical levels than z-level models. Both POM and ROMS have been used for modelling internal tides (POM: Holloway 1996, Robertson 2001a, ROMS: R. Hetland personal communication 2001). ROMS was chosen due to its use of a more accurate baroclinic pressure gradient formulation (density Jacobian scheme using monotonized cubic polynomial fits) (Ezer *et al.* 2002) and inclusion of thermobaric effects.

Several different numerical options are available in ROMS to simulate the different physical processes. In these simulations, third order upstream differencing for horizontal advection, Laplacian lateral diffusion along sigma surfaces (10 m^2 s^{-1}) (Shchepetkin & McWilliams in press), and the Large-McWilliams-Doney vertical mixing scheme were used (Large & Gent 1999). Radiative boundary conditions were implemented for the barotrophic mode velocities and flow relaxation boundary conditions for the baroclinic mode velocities and tracers. Tidal forcing

https://doi.org/10.1017/S0954102003001044 Published online by Cambridge University Press

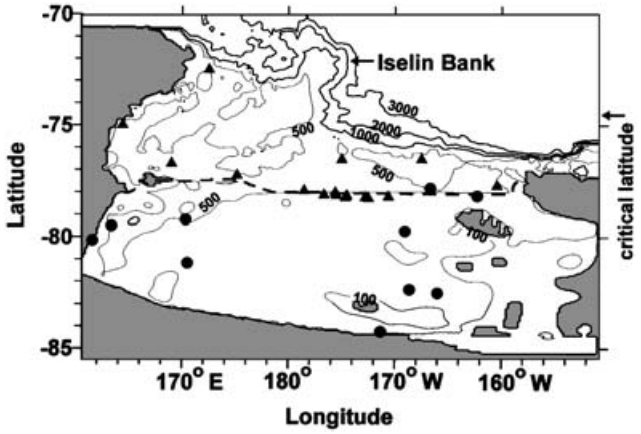


Fig. 1. The model domain with the water column thickness contoured at 100, 500, 1000, 2000, and 3000 m. The Ross Ice Shelf edge is indicated by a dashed line. The locations of tidal elevation observations are indicated by dots and those of velocity observations by triangles.

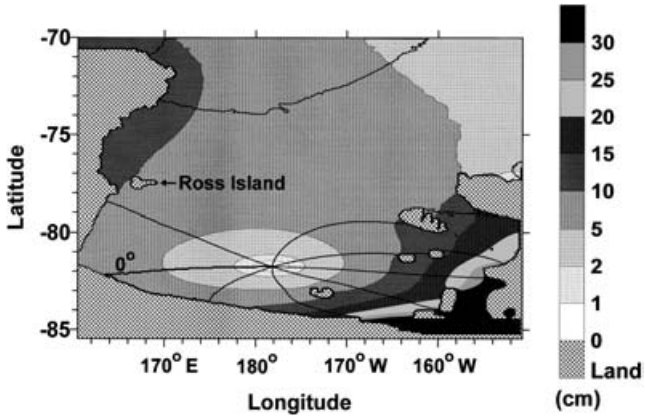


Fig. 2. The amplitude of the M_2 tidal elevation contoured at 1, 2, 5, 10, 15, 20, 25, and 30 cm. The overlaid heavy lines indicate the phase for the elevation, with the zero phase line indicated.

was implemented by setting elevations along all the open boundaries, with the coefficients taken from a two-dimensional model of the region ((CATS-99) Padman & Kottmeier 2000). Only one tidal constituent, the semi-diurnal M_2, was used. The barotrophic and baroclinic mode time steps were 8 s and 240 s, respectively, and the simulations were run for 17 days, with hourly data from the last two days used for analysis.

Topography and hydrography

For the Ross Sea, ROMS was modified to include the presence of an ice shelf. The ice shelf was assumed to be floating. Both mechanical and thermodynamic effects were included following Robertson (1999, 2001a) and Hellmer & Olbers (1989), respectively.

The model domain (Fig. 1) covered the Ross Sea with a spacing of 0.045° in latitude, 0.186° in longitude, and 24 vertical levels. North of 78°S, the water column thickness, the distance between the bottom and the ocean surface (or ice shelf base), was taken from Smith & Sandwell (1997). South of 78°S and under the ice shelf, the water column thickness and ice shelf thickness were supplied by Greischar *et al.* (1992 (electronic version also from Greischar)). Neither the water column nor the ice shelf thicknesses were smoothed. The minimum water column thickness was set to 50 m, which entailed artificially deepening portions of the region under the ice shelf, particularly near the eastern grounding line.

Initial potential temperature, θ, and salinity, S, fields were assembled from the World Ocean Circulation Experiment (WOCE) Hydrographic Programme Special Analysis Center (Gouretski & Jancke 1999), except under the ice shelf. Here, the hydrography was essentially a four layer system based on a θ and S profile through the ice shelf at a single location (J9 (Jacobs 1989)). The uppermost layer was 40 m thick with θ = the freezing point of water at the depth of the ice shelf base and S =34.39 psu. The second layer was 100 m thick with θ 0.06°C warmer than the freezing point of water for the depth. θ increased linearly between this value and that of the lowermost layer within the 50 m thick third layer. The lowermost layer encompassed the

Table I. Elevation amplitudes and phases from ROMS compared against observational data and other two-dimensional models. Underlined values for the amplitude exceed the observational uncertainty.

Location		Amplitude (cm)				Phase (°)			
Latitude	Longitude	Observations	ROMS	MacAyeal (1984)	Padman *et al.* (2000)	Observations	ROMS	MacAyeal (1984)	Padman *et al.* (2000)
84°15.0'S	171°19.8'W	8 ± 2	18	16	5	258	273	13	56
82°31.8'S	166°0.0'W	8 ± 2	11	7	9	213	202	290	209
82°22.2'S	168°37.8'W	7 ± 2	7	4	8	205	202	282	196
81°11.4'S	170°30.0'E	3 ± 2	5	6	6	310	21	117	160
80°11.4'S	161°33.6'E	5 ± 2	7	15	7	130	27	209	165
79°45.0'S	169°3.0'W	3 ± 2	7	8	9	75	95	187	147
79°31.8'S	163°38.4'E	4 ± 2	8	8	6	340	36	128	165
79°15.0'S	170°19.8'E	3 ± 2	7	7	6	300	49	136	160
78°12.0'S	162°16.2'W	3 ± 2	8	9	10	35	72	162	113
77°51.0'S	166°39.6'E	4 ± 2	9	8	4	6	57	147	164

https://doi.org/10.1017/S0954102003001044 Published online by Cambridge University Press

remaining water column (deeper than 190 m below the ice shelf base) with θ =-1.87°C and S =34.83 psu. S increased linearly between values in the uppermost and the lowermost layers over the 150 m of the middle two layers. The model elevation and velocities were initialized with the geostrophic velocities associated with the initial hydrography as determined from a simulation without tidal forcing.

Model outputs

Elevation, η, and depth-independent velocities, U_2 and V_2, are produced by the two-dimensional (barotrophic) mode of the model and θ, S, and depth-dependent velocities, U_3, V_3, and W_3, by the three-dimensional (baroclinic) mode. Foreman's tidal analysis routines were used to analyse these fields (Foreman 1977, 1978).

Results and discussion

Elevations and depth-independent velocities

The dominant feature of the M_2 tidal elevation amplitude is the amphidromic point located at *c*. 178°W, 82°S (Fig. 2). This amphidromic point results from overlap of the semidiurnal tide, which is *c*. 180° out of phase on opposite sides of the Ross Basin under the ice shelf, and is dependent on the relative size of the Ross Basin and the tidal wavelength (MacAyeal 1984). The M_2 tidal elevation amplitudes in the Ross Sea were generally small, ≤ 5 cm, although values > 10 cm were reached under the ice shelf, particularly the eastern portion, and along the western margin, north of Ross Island.

To evaluate the performance of the model, the modelled elevation amplitudes and phases were compared to those of the existing observations (Table I), whose locations are shown as dots in Fig. 1. The model elevation amplitudes were generally higher than the observations by 2–4 cm with seven of the ten values exceeding the observational uncertainty, 2 cm (Williams & Robinson 1980) (Table I). The largest discrepancy, 10 cm, occurred at the southern grounding line. The phases did not agree as well, with only half of the points agreeing within 45° (Table I). The phase changes rapidly in the vicinity of the amphidromic point and even a small error in the location of this point can result in significant errors in the phases.

For two major reasons, most of the differences between the observations and the model estimates are believed to be a result of topographic errors. First, the bathymetry and ice shelf thickness under the Ross Ice Shelf are not well known

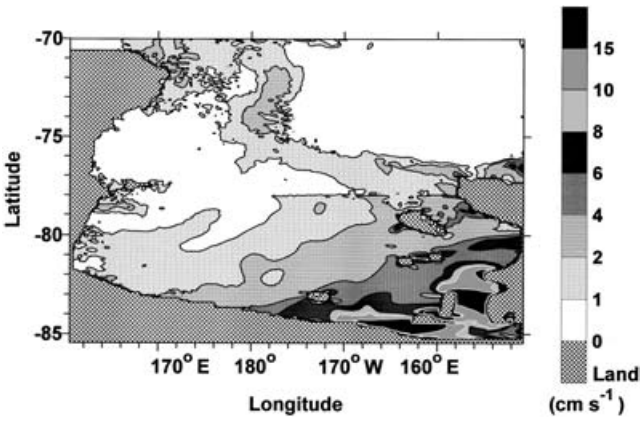


Fig. 3. The major axes of the M_2 tidal ellipses for the depth-independent velocities, contoured at 1, 2, 4, 6, 8, 10, and 15 cm s^{-1}.

Table II. Major axes of the M_2 tidal ellipses from ROMS compared against observational data. Underlined values for the amplitude exceed the observational uncertainty (1.7 cm s^{-1}).

Latitude	Longitude	Water depth (m)	Instrument depth (m)	ROMS (cm s^{-1})	Observation (cm s^{-1})
78°13.62'S	172°29.40'W	420	211	2.4	0.7
			283	2.9	0.8
			383	3.1	0.5
78°13.20'S	172°31.08'W	443	215	2.5	0.4
			291	1.2	1.0
			395	1.6	0.4
78°11.52'S	172°48.00'W	436	240	1.3	0.2
			315	1.0	1.0
			390	1.9	0.2
78°10.98'S	174°39.00'W	530	237	1.6	0.5
			310	2.3	0.1
			492	5.2	0.5
78°9.78'S	170°36.72'W	558	228	3.2	0.5
			305	3.7	0.4
78°6.48'S	174°30.78'W	567	210	1.1	0.4
			285	2.7	0.4
78°5.88'S	175°30.18'W	558	125	1.1	0.4
			225	1.5	0.4
			300	2.2	0.4
78°5.52'S	175°30.00'W	550	253	1.2	0.9
			327	2.2	0.3
			508	2.7	0.3
78°4.68'S	176°39.48'W	595	220	1.4	0.6
			425	1.7	0.4
77°58.68'S	175°35.82'W	585	210	1.0	0.5
			285	0.6	0.4
			515	1.3	0.3
77°52.92'S	178°31.98'W	700	340	0.3	0.3
			425	1.3	0.4
			650	1.3	0.4
77°40.80'S	160°24.18'W	590	255	1.8	0.9
			540	1.0	0.7
77°12.42'S	175°9.30'E	685	175	1.3	0.1
			350	1.0	0.3
76°30.093'S	167°29.971'W	775	241*	1.9	0.3, 0.1
			740*	1.9	0.4, 0.3
76°29.808'S	174°59.595'W	569	241*	1.0	0.8, 0.1
			534	1.0	39.23
74°57.90'S	164°23.58'E	879	40	1.2	0.6
			780	1.2	0.3
72°28.813'S	172°31.470'E	533	241	2.9	2.7
			498	2.9	6.9

* indicates sites where subsequent current observations were made.

https://doi.org/10.1017/S0954102003001044 Published online by Cambridge University Press

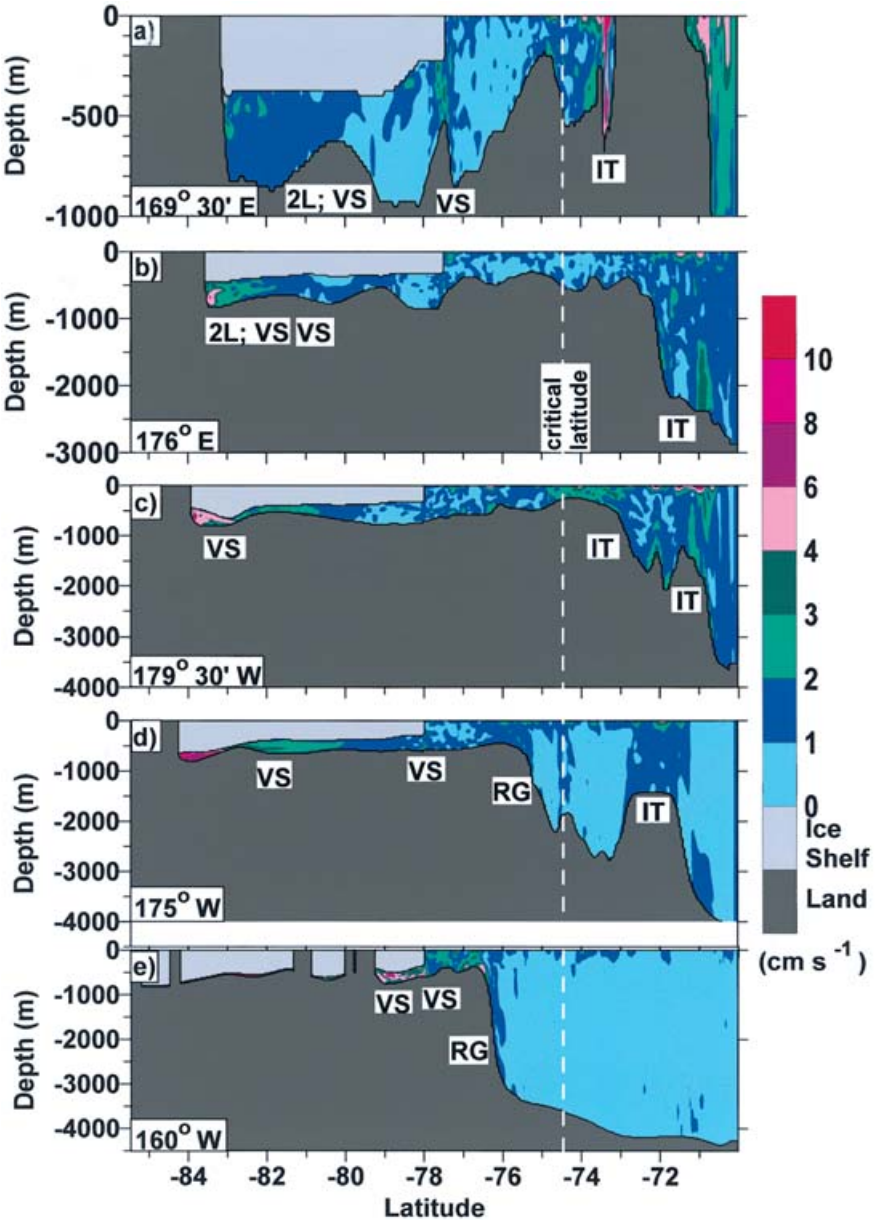


Fig. 4. The major axes of the tidal ellipses from the depth-dependent velocities along N–S transects at **a.** 169°30'E, **b.** 176°E, **c.** 179°30'W, **d.** 175°W, and **e.** 160°W. The pairs of letters indicate points discussed in the text (IT = internal tides, RG = reduced generation, VS = vertical shear, 2L = two-layer response). The location of the critical latitude is indicated by a dashed line.

and the model results are quite sensitive to errors in their estimates. Second, the artificial increase in the water column thickness reduced the bottom friction and dissipated less of the tidal energy, particularly at the back of the ice shelf. This not only had the effect of increasing the elevation, but also the group speed of the tidal Kelvin wave, consequently modifying the location of the amphidromic point. This effect has been previously seen in model results (MacAyeal 1984, Robertson *et al*. 1998, Padman *et al.* 1999). The incorrect position of the amphidromic point accounted for much of the discrepancy between the observations and the model results, particularly in the phases.

The model estimates were also compared to the results of two different two-dimensional tidal models (MacAyeal 1984, Padman & Kottmeier 2000). Padman's model (CATS-99 grid spacing: *c*. 6 km in longitude and *c*. 9 km in latitude) performed similarly to ROMS; however, MacAyeal's model (grid spacing: *c*. 10 km in longitude and *c*. 10 km in latitude) showed slightly less agreement. ROMS had significantly better phase agreement that the other two models (Table I). All models use slightly different topography explaining many of the differences between them.

The largest major axes of the tidal ellipses for the depth-independent velocities occurred in the south-west corner of the ice shelf cavity (Fig. 3). Elsewhere, the major axes were generally quite small, less than 4 cm s^{-1}. The velocities increased along the continental slope and high values occurred over the Iselin Bank. Again the topography was the primary controlling factor for the depth-independent velocities, as has been previously noted for a two-dimensional tidal model (Robertson *et al*. 1998).

https://doi.org/10.1017/S0954102003001044 Published online by Cambridge University Press

Thus the model simulated reasonably well the major features of the observed barotrophic tidal flow in the Ross Sea. The differences between the model estimates and the observations were primarily attributable to lack of detailed topographic data for the ice shelf cavity.

Depth-dependent response

To evaluate further the response of the model, the major axes of the tidal ellipses for depth-dependent velocities were compared to those of forty-two current meters on seventeen moorings, whose locations are shown as triangles in Fig. 1. The model estimates for the major axes were generally larger than the observed values (Table II), but were within the observational uncertainty of 1.7 cm s^{-1} (Pillsbury & Jacobs 1985) for twenty-nine of the forty-two sites. At two locations over Iselin Bank, the observations reported extremely high tidal benthic velocities (bottom values at 76°29.808'S, 72°28.813'S in Table II), which were not seen in the model results. These may be locally high values and are probably a result of small-scale topographic features irresolvable with the model topography. The high observational values could be an inertial response, but their location near the bottom and their strong depth dependence reduce this possibility. Another possible explanation for the high observational values is that they are a first harmonic response from the diurnal constituents, which induce continental shelf waves in this region. The higher values of the model estimates are again attributed to the lack of accurate, high resolution topographic data and the higher group wave speed resulting from the limit on the water column thickness.

The M_2 critical latitude, 74°28.8'S, crosses through the domain (Fig. 1 and dashed line in Fig. 4). At the critical latitude the inertial frequency equals the tidal frequency. This affects both the generation and propagation of internal tides. Linear internal wave theory predicts that internal waves will not be generated nor propagate poleward of the critical latitude. Robertson (2001a) gives a more extensive explanation of the relevant linear internal wave theory.

Generation and propagation of internal tides occurred over the continental slope and steep topography equatorward of the critical latitude (areas indicated with IT in Fig. 4a–d), especially in the western Ross Sea (Fig. 4a–c), where the continental slope is equatorward of critical latitude (Fig. 1). In the eastern Ross Sea, east of 174°W, the continental slope is poleward of the critical latitude (Fig. 1) and the generation of internal tides is reduced (areas marked RG in Fig. 4d & e). The internal tides showed the expected wavelengths and propagated along the expected wave characteristics according to linear internal wave theory.

Strong vertical shears in the horizontal velocities are an indicator of potential mixing. They occurred under and at the front of the ice shelf (areas marked VS in Fig. 4a–f). Although the existence of internal tides is not expected in a continuously stratified fluid according to linear internal wave theory, it is quite possible for a baroclinic mode tide to exist in the multiple layer system (Kundu 1990, p. 233), such as that of the initial hydrographical conditions in the ice cavity. A two layer response is apparent under the ice shelf with the upper two layers (140 m) essentially responding together as the top layer and the lowermost layer as the bottom layer (area marked 2L in Fig. 4a & b). Additionally, strong vertical shears in the horizontal velocities occurred in the regions of internal tide generation (areas marked IT in Fig. 4a–e).

Implications of model results

Lead formation due to tidal divergence can affect the ocean-atmosphere heat flux. Since the heat flux increases by 1–2 orders of magnitude over leads compared to an ice covered ocean (Maykut 1986), a lead formation percentage of 1–10% would significantly increase the ocean-atmosphere heat flux. Mean lead formation percentages, $L_{\%}$, were estimated from the "Eulerian" divergence of both the depth-independent velocities and the depth-dependent surface velocities according to

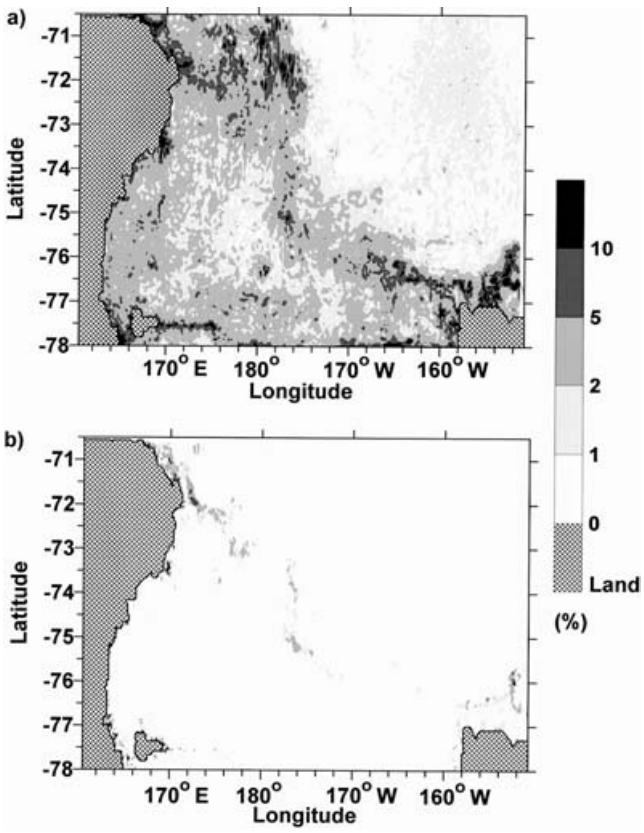


Fig. 5. Lead formation estimates from **a.** the depth-dependent surface velocities and **b.** the depth-independent velocities. Contours are shown at 1, 2, 5, and 10%.

https://doi.org/10.1017/S0954102003001044 Published online by Cambridge University Press

$$L\% = 0.5\left[0.5\mathrm{T}\left\langle \nabla \cdot \mathbf{V} \right\rangle\right] \quad (1)$$

where T is the tidal period (44,712 s for M_2), $\nabla \cdot \boldsymbol{V}$ is the divergence of either the depth-independent velocities or the depth-dependent surface velocities (i.e. $\nabla \cdot \boldsymbol{V} = \partial U_2/\partial x + \partial V_2/\partial y$ or $= \partial U_3/\partial x + \partial V_3/\partial y$, respectively) and angle brackets indicate the standard deviation of the quantity. High lead formation percentages occurred over steep topographic changes along the continental shelf break (Fig. 5). The estimate of lead formation increased by a factor of 2–5 for the depth-dependent surface velocities compared to the depth-independent velocities (Fig. 5a & b). These crude estimates are likely to be an upper bound, since they do not include effects of the ice motion on the ocean dynamics or damping or blockage of the ice motion. Lead formation percentages of 5–10% have been observed over the continental slope in the western Weddell Sea (C.A. Geiger, personal communication 2002), indicating that although these values are high, they are realistic as an upper bound. Additionally, only one tidal constituent was used in these estimates and estimates using multiple constituents will be different due to constructive and destructive interference between the constituents. Despite the caveats, these rough estimates indicate that tides can significantly increase the ocean-atmosphere heat transfer.

Acknowledgements

Thanks are due to E. Curchitser, H. Garcia, and A. Shchepetkin for assistance with ROMS and helpful discussions on inclusion of the ice shelf. We would like to thank Andrey Proshutinsky and Laurie Padman for their insightful and well appreciated comments and efforts reviewing the paper. This study was funded by grant INT-0000394 from the National Science Foundation (NSF) with publication fees paid by (Office of Polar Programs) OPP grant OPP-00-3425. Additionally, the Alfred-Wegener-Institut für Polar- und Meeresforschung provided support for A. Beckmann and H. Hellmer and computer equipment and office space for R. Robertson. This is Lamont publication 6349. Any opinions, findings, and conclusions or recommendations expressed in this material are those of the authors and do not necessarily reflect the views of the National Science Foundation.

References

Beckmann, A., Timmermann, R., Pereira, A.F. & Mohn, V. 2001. Sea ice anomalies in the eastern Weddell Sea. *CLIVAR Exchanges*, **6**, 15–16.

Ezer, T., Arango, H. & Shchepetkin, A.F. 2002. Developments in terrain-following ocean models: Intercomparisons of numerical aspects. *Ocean Modeling*, **4**, 249–267.

Foreman, M.G.G. 1977. *Manual for tidal height analysis and prediction*. Pacific Marine Science Report No. 77–10. Sidney, Canada: Institute of Ocean Sciences, 58 pp.

Foreman, M.G.G. 1978. *Manual for tidal current analysis and prediction*. Pacific Marine Science Report No. 78–6, Sidney, Canada: Institute of Ocean Sciences, 70 pp.

Gouretski, V.V. & Jancke, K. 1999. A description and quality assessment of the historical hydrographic data for the South Pacific Ocean. *Journal of Atmospheric and Oceanic Technology*, **16**, 1791–1815.

Greischar, L.L., Bentley, C.R. & Whiting, L.R. 1992. An analysis of gravity measurements on the Ross Ice Shelf, Antarctica. *Antarctic Research Series*, **57**, 105–155.

Hellmer, H.H. & Olbers, D.J. 1989. A two-dimensional model for the thermohaline circulation under an ice shelf. *Antarctic Science*, **4**, 325–326.

Holloway, P.E. 1996. A numerical model of internal tides with application to the Australian northwest shelf. *Journal of Physical Oceanography*, **26**, 21–37.

Jacobs, S.S. 1989. Marine controls on modern sedimentation on the Antarctic continental shelf. *Marine Geology*, **85**, 121–153.

Kundu, P.K. 1990. *Fluid mechanics*. San Diego, CA: Academic Press, 638 pp.

Large, W.G. & Gent, P.R. 1999. Validation of vertical mixing in an equatorial ocean model using large eddy simulations and observations. *Journal of Physical Oceanography*, **29**, 449–464.

MacAyeal, D.G. 1984. Numerical simulation of the Ross Sea tide. *Journal of Geophysical Research*, **89**, 607–615.

Maykut, G.H. 1986. The surface heat and mass balance. *In* Untersteiner, N., *ed*. *Geophysics of sea ice*. New York: Plenum Press, 395–463.

McPhee, M.G., Ackley, S.F., Guest, P., Huber, B.A., Martinson, D.G., Morison, J.H., Muench, R.D., Padman, L. & Stanton, T.P. 1996. The Antarctic flux zone experiment. *Bulletin of the American Meteorological Society*, **77**, 1221–1232.

Muench, R.D., Padman, L., Howard, S.L. & Fahrbach, E. 2002. Upper ocean diapycnal mixing in the northwestern Weddell Sea. *Deep-Sea Research II*, **49**, 4843–4862.

Munk, W. & Wunsch, C. 1998. The moon and mixing: abyssal recipes II. *Deep-Sea Research*, **45**, 1977–2010.

Nansen, F. 1898. *Farthest north*, vol. 1. London: George Newnes, 510 pp.

Padman, L. & Kottmeier, C. 2000. High-frequency ice motion and divergence in the Weddell Sea. *Journal of Geophysical Research*, **105**, 3379–3400.

Padman, L., Robertson, R. & Nicholls, K. 1999. Modeling tides in the southern Weddell Sea: updated model with new bathymetry from ROPEX. *Filchner–Ronne Ice Shelf Programme*, **12**, 65–73.

Padman, L., Erofeeva, S. & Joughin, C. 2003. Tides of the Ross Sea and Ross Ice Shelf cavity. *Antarctic Science*, **15**, 31–40.

Pillsbury, R.D. & Jacobs, S.S. 1985. Preliminary observations from long-term current meter moorings near the Ross Ice Shelf, Antarctica. *Antarctic Research Series*, **43**, 87–107.

Robertson, R. 1999. *Mixing and heat transport mechanisms for the upper water column in the Weddell Sea*. PhD thesis, College of Oceanic and Atmospheric Sciences, Oregon State University, 190 pp. [Unpublished].

Robertson, R. 2001a. Internal tides and baroclinicity in the southern Weddell Sea: Part I: Model description, and comparison of model results to observations. *Journal of Geophysical. Research*, **106**, 27001–27016.

Robertson, R. 2001b. Internal tides and baroclinicity in the southern Weddell Sea: Part II: Effects of the critical latitude and stratification. *Journal of Geophysical. Research*, **106**, 27017–27034.

Robertson, R., Padman, L. & Egbert, G.D. 1998. Tides in the Weddell Sea. *Antarctic Research Series*, **75**, 341–369.

Shchepetkin, A.F. & McWilliams, J.C. In press. A method for computing horizontal pressure gradient force in an ocean model with non-aligned vertical coordinate. *Journal of Geophysical Research.*

Smith, W.H.F. & Sandwell, D.T. 1997. Global seafloor topography from satellite altimetry and ship depth soundings. *Science*, **277**, 1956–1962.

Williams, R.T. & Robinson, E.S. 1980. The ocean tide in the southern Ross Sea. *Journal of Geophysical Research*, **85**, 6689–6696.

https://doi.org/10.1017/S0954102003001044 Published online by Cambridge University Press